The Prospect of Mixed Rare Earth Barium Copper Oxides

Kai Walter, Manuela Erbe, Jens Hänisch, and Bernhard Holzapfel

***Abstract*—To improve the superconducting properties of Rare Earth Barium Copper Oxides (REBCO) for applications at low temperatures and high fields, the defect landscape of lower-dimensional defects needs to be optimized. This can be achieved by forming solid solutions of various REBCO phases, so called mixed REBCO systems (mREBCO), which are characterized by disorder at the RE position depending on the used RE elements. These RE elements also determine the lattice parameters of the resulting mREBCO compound. Thereby, mREBCO thin films offer the opportunity to study *RE* mixing in deliberately tuned crystal structures. In order to investigate the influence of *RE* mixing on the superconducting properties, sets of mREBCO thin films were produced by chemical solution deposition. As these investigations show, the mean ionic RE radius of mREBCO thin films can be used to predict their lattice parameters. Therefore, the crystal structure of mREBCO compounds makes it possible to adapt the films to different substrates or buffer layers. It had been reported that *RE* mixing increases the microstrain along the *c*-axis, yet our sample sets showed a significant decrease with *RE* mixing, possibly due to different growth conditions. Surprisingly, the mREBCO sample sets showed no significant change of the weak-pinning contribution, which is associated with point-like defects. Yet the pinning force was positively influenced by *RE* mixing.**

***Index Terms*—Ionic radius, mixed REBCO, mREBCO, pinning, XRD.**

I. Introduction

RESEARCH attention around the topic of mixing *RE* within REBCO crystal structures gained new interest in the last couple of years as so-called "high-entropy" REBCO, of which especially epitaxial thin film samples have shown promising results in terms of pinning at low temperatures and high magnetic fields [1], [2]. Changes in pinning behavior due to an increased entropy of mixing were identified by Yamashita et al. [3], [4], and Chen et al. [5] have measured increasing microstrain along the *c*-axis with increased entropy of mixing. These works show the potential of *RE* mixing, yet the mechanism of how *RE* mixing improves the pinning behavior of REBCO thin films still remains shrouded.

From here on out, "high-entropy" REBCO will be called mixed REBCO (mREBCO), because the term "high-entropy" should be reserved for actual high-entropy compounds, as we believe that a statistical distribution of *RE* on only one site does not constitute a high-entropy compound. Additionally, only one of our sample sets would satisfy the softened definition of high-entropy compounds (at least 5 constituents). Other authors circumvented this predicament by naming their samples "high-entropy-like REBCO". While this term is technically more correct, it is also quite cumbersome. Hence, we will be using the term mixed REBCO.

For the scope of this work, Chemical Solution Deposition (CSD) was used to prepare the mREBCO thin films. CSD offers the opportunity to study a wide range of mREBCOs by simply mixing the stock solutions of each *RE* proportionally. We prepared five solutions to produce thin films with the same mean ionic radius but with increasing variance in r(RE) to investigate the effects of variance on the microstructure and pinning behaviour.

II. Experimental Methods

Mixed REBCO thin films were prepared by CSD using trifluoroacetate metal organic deposition solutions based on methanol as a solvent. Stock solutions of each *RE* with a ratio of 1:2:3 for *RE*, Ba and Cu ions and a total molar cation amount of 1.5 mol l^{-1} were produced and mixed in the ratios given in Table I. The solution chemistry is described in greater detail in Ref. [6]. The ratios were chosen so that the mean *RE* radius, $\bar{r}(RE)$, remained constant while the variance of *r*(*RE*), *var*(*r*(*RE*)), increased across the solutions. The variance was calculated according to:

$$var\left(r\left(RE\right)\right) = \sum_{i=1}^{n} f_i \cdot \left(r(RE)_i - \bar{r}\left(RE\right)\right)^2, \qquad (1)$$

where f_i and $r(RE)_i$ denote the normed ratio and ionic radius of each RE ion for a given solution.

The solutions were spin-coated onto cleaned 10 × 10 mm^2 [100]-oriented $LaAlO_3$ (LAO) single crystal substrates to achieve a film thickness of approx. 200 nm. After coating, these samples were pyrolyzed and crystallized. The 1RE and 2RE samples crystallized at 810 °C and a $p(O_2)$ of 150 ppm according to the optimum conditions of Erbe et al. [7]. For the crystallization of the remaining samples, we found a temperature gradient from 805 to 820 °C and a low $p(O_2)$ of 50 ppm to facilitate c-axis growth as optimal conditions due to the different optimal conditions of the single-RE phases [7]. The oxygenation was kept constant for all sample sets. All thin films were oxygenated

TABLE I
OVERVIEW OF USED SOLUTIONS WITH THEIR RESPECTIVE *RE*-RATIOS AS WELL AS THEIR MEAN *RE* RADIUS *r* AND VARIANCE

solution	**ratio**							**mean $r(RE)$ / Å**	***var*($r(RE)$) / 10^{-5} Å^2**
	Er	Ho	Dy	Gd	Eu	Sm	Nd		
1RE				1				1.530	0
2RE			1		2			1.530	34
3RE			1.5		1	1		1.530	53
4RE	1	1			2	2.35		1.530	91
5RE	1	1			1.55	1.5	0.5	1.530	127

at 450 °C for 2 h with a subsequent furnace cooling in flowing O_2.

The lattice parameters of the thin film samples were determined using a Rigaku Smartlab 3kW. Monochromatic Cu K_α radiation at 40 kV and 30 mA was used in parallel-beam geometry to minimize sample misalignment. The lattice parameter *c* was determined from $\theta/2\theta$ scans following the Nelson-Riley Method [8] using all available (00*l*) peaks between 5° and 120°. The lattice parameters *a* and *b* were determined using the (30<u>10</u>)/(03<u>10</u>) and (136)/(316) peak pairs, see Ref. [9] for more details.

The superconducting properties were investigated using a 14-T Quantum Design PPMS. Inductive measurements were carried out with a self-designed and calibrated mutual inductance device to characterize the superconducting transition using the values T_c^{90} and T_c^{10}, which were defined as the temperatures at which the measured voltage was 90% and 10% of the normal-state value. The sharpness of the transition can thereby be defined as $\Delta T_c = T_c^{90} - T_c^{10}$.

The critical current density, J_c, was determined using resistively-measured *U*(*I*) curves. $J_c(B)$ measurements were used to determine the pinning force density F_p. J_c was measured at magnetic fields *B* from 0 to 14 T at 77, 50 and 30 K. Only the normalized F_p plot for 77 K is presented in this work due to length limitations. $J_c(T)$ measurements were done to analyze the weak and strong pinning contributions. Thus, J_c was measured from 90 K down to 5 K at 0.5, 1, 3 and 5 T. The resulting $J_c(T)$ curves were fitted using the sum of the weak and strong pinning contributions [10], [11]:

$$\text{weak}: \; J_c^{\text{wk}}(T) = J_c^{\text{wk}}(0) * \exp\left(-\frac{T}{T_0}\right) \quad (2)$$

$$\text{strong}: \; J_c^{\text{str}}(T) = J_c^{\text{str}}(0) * \exp\left(-3\left(\frac{T}{T^+}\right)^2\right), \quad (3)$$

in which $J_c^{\text{wk}}(0)$ and $J_c^{\text{str}}(0)$ are the weak and strong pinning contributions at 0 K, and T_0 (∼5–15 K) and T^+ (∼70–90 K) are the corresponding characteristic thermal energies of vortex pinning expressed as temperatures at these defects respectively [11].

III. RESULTS AND DISCUSSION

In order to study the influence of *RE* mixing in mREBCO thin films, five sets of samples were prepared. The ratios were chosen a priori in an attempt to yield crystal structures with the same mean lattice parameters as GdBCO, the 1RE sample set, and varying amounts of disorder from *RE* mixing.

Producing mREBCO thin films comes with challenges, as each individual REBCO system has its own optimal CSD processing window. The crystallization temperature, T_{cryst}, and partial pressure of oxygen, $p(O_2)$, are especially important [12]. T_{cryst} must be high enough to avoid *a*-axis growth and low enough to avoid the formation of rare-earth oxides (REO), which become more stable at higher temperatures. The oxygen partial pressure further influences the growth speed of *c*- and *a*-axis oriented REBCO and REOs. For the 3RE, 4RE and 5RE, a T_{cryst} gradient was used to accommodate for the wide range of optimal T_{cryst}, and $p(O_2)$ was set to 50 ppm to reduce the amount of REO formation as much as possible. This approach proved successful as most samples had low amounts of *a*-axis growth and REO formation, Fig. 1(a). The sets showed comparably high degrees of crystallinity except for the 5RE samples. Judging from the integral intensity of the (30<u>10</u>)/(03<u>10</u>) peak pairs, the crystallinity of the 5RE sample set varied significantly, with the best samples still having the same integral intensity and thus crystallinity as all other sample sets, Fig. 1(b). These samples, with a mean $J_c^{\text{sf}}(77\text{K})$ ranging from 3.3 to 2.5 MAcm^{-2} for the 1RE to 5RE sample set, were used for the resistive measurements to insure comparability.

The lattice parameters *a* and *b* of all sample sets agree very well with the target values of thin film GdBCO (gray dotted lines), Fig. 2(a). The lattice parameters *c* scatter around the target value. Values higher than expected can be explained by differing oxygenation states, as the lattice parameter *c* increases for increasing oxygen deficiency δ [6]. The lattice parameters *c* of the 5RE sample set were consistently smaller than expected. This is most likely caused by over-proportional incorporation of smaller *RE* into the thin film and larger *RE* preferably forming REOs. Transmission electron microscopy is needed to clarify this point.

T_c^{90} decreases from ∼94.5 to 93.3 K with increasing *RE* mixing, Fig. 2(c). Fig. 2(b) shows that the superconducting transition, ΔT_c, slightly broadens with *RE* mixing. This is to be expected as T_c fluctuations are created by the statistical *RE* distribution throughout the thin film and thereby widening the superconducting transition. It may therefore be concluded that the CSD mixing method can be used to produce mREBCO thin films reliably, whilst tuning their lattice parameters. This way, tailoring the crystal structure to different substrates or buffer layers becomes considerably easier.

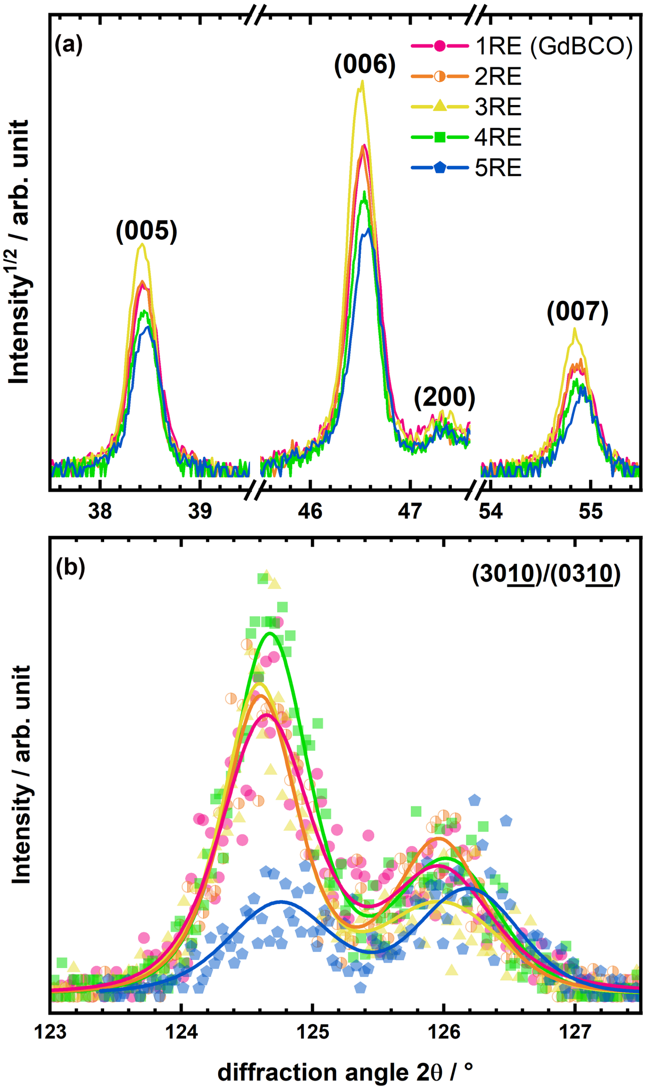

Fig. 1. Representative XRD results of all sample sets. (a) (005), (006), (007) peaks from $\theta/2\theta$ scans. A region of low interest (39.5-45.5°) and the LAO substrate peak (47.5-54°) were cut out to improve readability. A small *a*-axis, (200), peak was found for all samples, indicating non-optimal growth conditions. (b) (30<u>10</u>)/(03<u>10</u>) peak pair due to twinning in the *ab*-plane. The integral intensity was comparable for all sample sets except 5RE, most likely due to worse crystallinity.

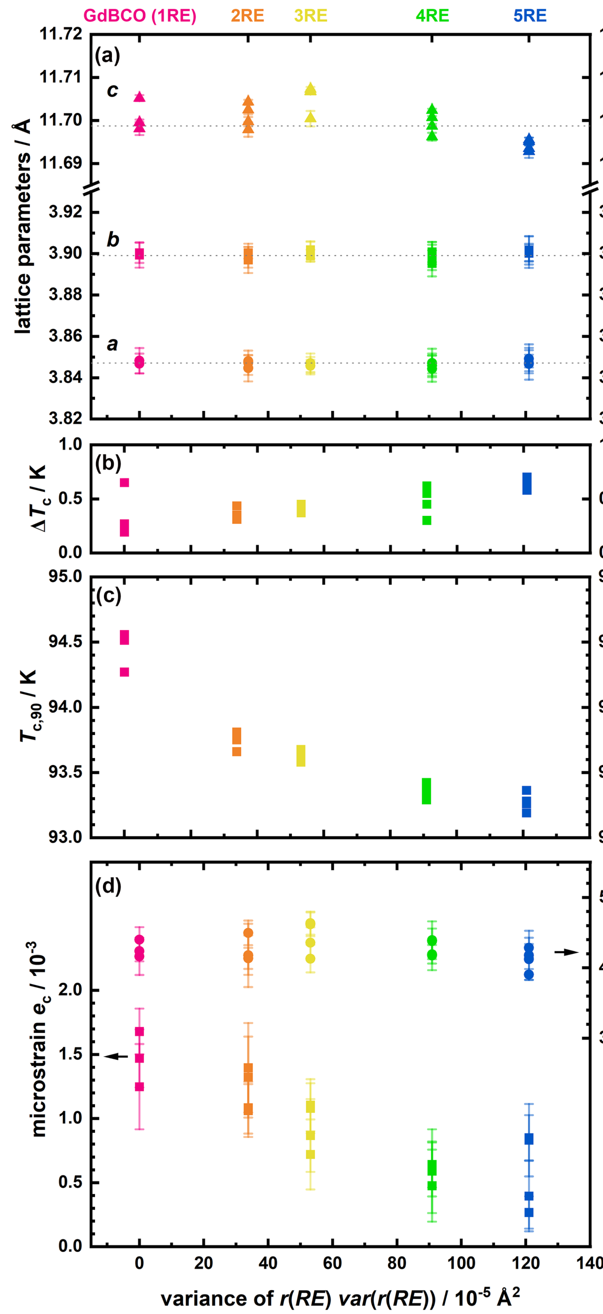

Fig. 2. Influence of the variance of *RE* radii *var*(*r*(*RE*))) on: (a) Lattice parameters. The dotted lines indicate the target values based on GdBCO. Characterization of the superconducting transition: (b) The sharpness of the transition expressed as ΔT_c. (c) T_c^{90} of the transition. (d) Microstrain e_c and crystallite size D_c along the c-axis. The error bars are one standard deviation. Each mREBCO sample set is characterized by a unique color, upper x-axis.

The microstrain e_c and crystallite size D_c along the *c*-axis can be determined from the integral widths β of $\theta/2\theta$ scans via Williamson-Hall analysis [9], Fig. 2(d). Here, e_c and D_c are plotted over the variance of *RE* radii, *var*(*r*(*RE*)). While D_c stays constant across all samples at around 43 ± 2 nm, the microstrain e_c changes significantly with *var*(*r*(*RE*)).

It had been reported that *RE* mixing may increase microstrain within CSD [5] and PLD [13] thin film samples. We found the opposite. As shown in Fig. 2(d), an increasing *var*(*r*(*RE*)) from *RE* mixing results in a significant reduction of e_c by ∼75%. One possible reason for this behavior might be the layer-by-layer growth of CSD thin films [14]. Another reason for the observed differences in CSD thin films between Chen et al. [5] and our study might be the fact that they combined *RE* mixing and *RE* over-doping so that their films had a stoichiometry of 1.5:2:3 for *RE*/Ba/Cu respectively.

RE mixing gives the growing lattice an additional degree of freedom with which it can reduce growth-related strain. Thus, the more *RE* ions of different sizes are available, the higher the reduction of e_c. Outliers at 5RE show about twice the amount of microstrain than the rest of the sample set. We believe that the increased microstrain is a result of the previously mentioned non-optimal growth conditions. The thin film quality varied a lot within the 5RE sample set. While the *RE* mixing gives the system an additional degree of freedom to reduce strain, it also adds more complexity to the growth process. A careful balance

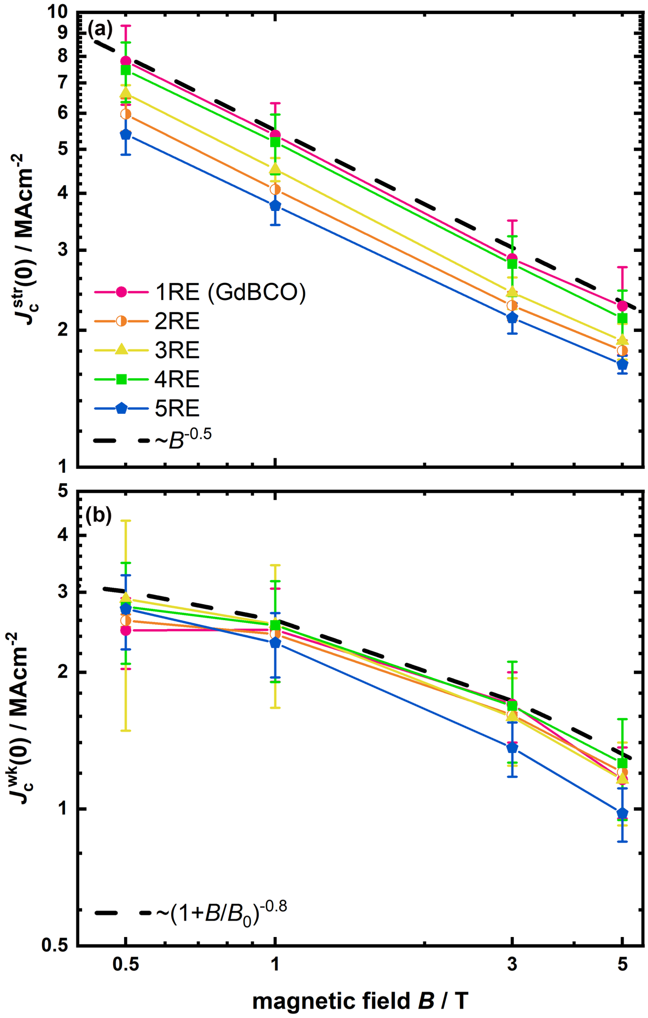

Fig. 3. Log-Log plot of the pre-exponential coefficients of the strong, (a), and weak, (b), pinning contributions. Shown are mean values of two samples for all sets. The error bars represent the full range of measured values. Dotted lines visualize the overall trend in each plot.

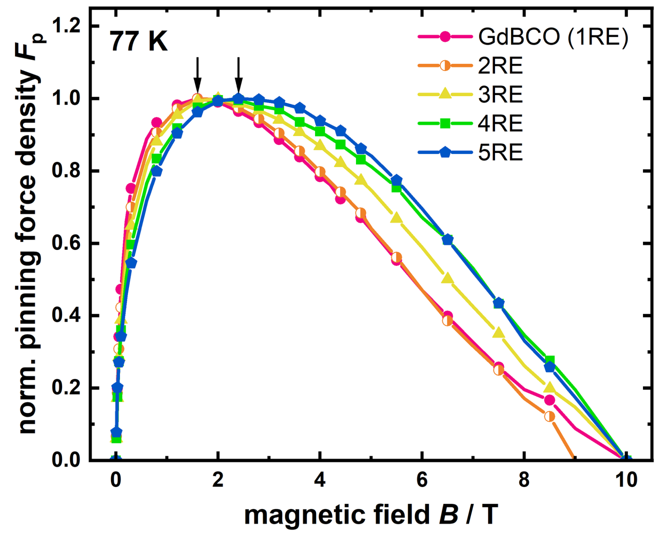

Fig. 4. Normalized pinning force density $F_{\rm p}$ at 77 K of all sample sets. The magnetic field of maximum $F_{\rm p}$, $B_{\rm max}$, is indicated with a black arrow for the 1RE and 5RE sample set. An increase from 1.6 to 2.4 T is visible. Only every 2nd data point is plotted for readability. The color code is inherited from previous figures.

must be reached between *RE* mixing and deposition complexity. The heat treatment conditions for all other mREBCO sets led to thin films of good crystallinity. We believe 5RE samples with comparable quality and low microstrain can be produced with more optimization.

RE mixing should introduce point-like defects. Their effect on the pinning behavior is captured in the weak pinning contribution. $J_{\rm c}$ was measured from 90 to 5 K at 0.5, 1, 3 and 5 T and fitted using the sum of (2) and (3) as described in Refs. [10], [11].

The strong pinning contribution $J_{\rm c}^{\rm str}(0)$, Fig. 3(a) followed $\sim B^{-q}$, q = 0.5. *RE* mixing did not influence how the pre-exponential factor decays with B. The highest absolute values were achieved with GdBCO followed by 4RE and 3RE samples. The 5RE samples performed the worst due to the aforementioned deposition difficulties. Nevertheless, $J_{\rm c}$ improvements for all mREBCO sets can be expected, as only minor optimizations have been made to the deposition conditions so far. The weak-pinning contribution $J_{\rm c}^{\rm wk}(0)$ behaved like $\sim(1+\frac{B}{B_0})^{-p}$, with $p = 0.8$, where B_0 denotes the crossover field for the transition from single vortex pinning to collective pinning [15]. Surprisingly, $J_{\rm c}^{\rm wk}(0)$ showed even less change than $J_{\rm c}^{\rm str}(0)$ due to *RE* mixing, Fig. 3(b). The weak-pinning contribution of all sample sets is mostly identical. This was unexpected, as *RE* mixing should introduce more point-like defects, which should increase $J_{\rm c}^{\rm wk}(0)$. Based on the presented data the initial hypothesis that RE mixing should improve $J_{\rm c}^{\rm wk}(0)$ must be refuted. Regardless, the presented samples will be further investigated at higher fields to determine whether fields up to 5 T were too small to measure any significant differences. Irrespective of this fact, it can be seen that the weak-pinning contribution decays more slowly with B than its strong counterpart.

While the investigation of the strong and weak pinning contributions suggests no significant difference between the sample sets, the pinning force density $F_{\rm p}$ shows qualitative changes even at 77 K. As clearly seen from Fig. 4, the field of maximum pinning force, $B_{\rm max}$, shifts from 1.6 to 2.4 T with increasing *RE* mixing, illustrating that the pinning behavior of mREBCO thin films has the potential to outperform 1RE systems at higher magnetic fields. It should also be noted that *RE* mixing possibly influences the formation of different pinning centers such as stacking faults, antisite defects etc. Thus, the observed changes might not be due to *RE* mixing directly, but a secondary effect of *RE* mixing by changing the existing pinning landscape.

This investigation showed that *RE* mixing with CSD allows for lattice parameter tailoring of mREBCO thin films. The resulting lattice parameters can be accurately predicted by using the mean ionic radius of the applied mREBCO solution. Secondly, *RE* mixing adds more complexity to the deposition process but enables the crystal lattice to reduce microstrain during growth. While this additional degree of freedom benefits the growth in general, more optimization within the used mREBCO systems must be done to achieve or even surpass the superconducting performance of already optimized 1RE systems, such as GdBCO in this study. The pinning analysis was non-conclusive. While the $J_c(T)$ investigations at fields up to 5 T did not show any significant changes, the normalized pinning force density at 77 K revealed that *RE* mixing improves the pinning behavior at higher magnetic fields. The full scope of the influence of *RE* mixing will be further investigated with optimizations of the deposition conditions, J_c measurements at magnetic fields up to 14 T and anisotropy investigations to identify whether *RE* mixing influences the iso- or anisotropic pinning contributions of mREBCO thin films.

References

[1] P. Cayado, L. Grünewald, M. Erbe, J. Hänisch, D. Gerthsen, and B. Holzapfel, "Critical current density improvement in CSD-grown high-entropy $REBa_2Cu_3O_{7-\delta}$ films," *RSC Adv.*, vol. 12, no. 44, pp. 28831–28842, 2022, doi: 10.1039/d2ra03807b.

[2] P. Cayado and J. Hänisch, "High-entropy superconducting materials," in *High Entropy Alloys - Composition and Microstructure Design [Working Title]*. London, U.K.: IntechOpen, 2024.

[3] A. Yamashita, Y. Shukunami, and Y. Mizuguchi, "Improvement of critical current density of $REBa_2Cu_3O_{7-\delta}$ by increase in configurational entropy of mixing," *Roy. Soc. Open Sci.*, vol. 9, no. 3, 2022, Art. no. 211874, doi: 10.1098/rsos.211874.

[4] A. Yamashita, "Pinning mechanism of mixed REBCO," *Private Commun.*, vol. 1, Sep. 2023, Art. no. e12.

[5] J. Chen et al., "Nucleation and epitaxy growth of high-entropy $REBa_2Cu_3O_{7-\delta}$ (RE = Y, Dy, Gd, Sm, Eu) thin films by metal organic deposition," *J. Rare Earths*, vol. 41, no. 7, pp. 1091–1098, 2023, doi: 10.1016/j.jre.2022.06.006.

[6] M. Erbe et al., "Improved $REBa_2Cu_3O_{7-x}$ (RE = Y, Gd) structure and superconducting properties by addition of acetylacetone in TFA-MOD precursor solutions," *J. Mater. Chem. A*, vol. 2, no. 14, 2014, Art. no. 4932, doi: 10.1039/c3ta15243j.

[7] M. Erbe et al., "Comparative study of CSD-grown RE BCO films with different rare earth elements: Processing windows and T_c," *Supercond. Sci. Technol.*, vol. 33, no. 9, 2020, Art. no. 94002, doi: 10.1088/1361-6668/ab9aa0.

[8] J. B. Nelson and D. P. Riley, "An experimental investigation of extrapolation methods in the derivation of accurate unit-cell dimensions of crystals," *Proc. Phys. Soc.*, vol. 57, no. 3, pp. 160–177, 1945, doi: 10.1088/0959-5309/57/3/302.

[9] K. Walter, M. Erbe, A. Welle, J. Hänisch, and B. Holzapfel, "Precise determination of oxygen content in $SmBa_2Cu_3O_{7-\delta}$ thin film samples using X-ray diffraction," *Supercond. Sci. Technol.*, vol. 37, no. 7, 2024, Art. no. 75002, doi: 10.1088/1361-6668/ad4a30.

[10] J. P. F. Feighan, A. Kursumovic, and J. L. MacManus-Driscoll, "Materials design for artificial pinning centres in superconductor PLD coated conductors," *Supercond. Sci. Technol.*, vol. 30, no. 12, 2017, Art. no. 123001, doi: 10.1088/1361-6668/aa90d1.

[11] T. Puig et al., "Vortex pinning in chemical solution nanostructured YBCO films," *Supercond. Sci. Technol.*, vol. 21, no. 3, 2008, Art. no. 34008, doi: 10.1088/0953-2048/21/3/034008.

[12] R. Hayasaka et al., "Investigation of the crystallization process of CSD-ErBCO on IBAD-substrate via DSD approach," *Sci. Reports*, vol. 10, no. 1, 2020, Art. no. 19934, doi: 10.1038/s41598-020-76848-y.

[13] A. Yamashita et al., "Fabrication of high-entropy $REBa_2Cu_3O_{7-\delta}$ thin films by pulsed laser deposition," *Jpn. J. Appl. Phys.*, vol. 61, no. 5, 2022, Art. no. 50905, doi: 10.35848/1347-4065/ac5b39.

[14] D. M. Feldmann, T. G. Holesinger, R. Feenstra, and D. C. Larbalestier, "A review of the influence of grain boundary geometry on the electromagnetic properties of polycrystalline $YBa_2Cu_3O_{7-x}$ films," *J. Amer. Ceram. Soc.*, vol. 91, no. 6, pp. 1869–1882, 2008, doi: 10.1111/j.1551-2916.2008.02273.x.

[15] A. Ballarino Succi, S. C. Hopkins, C. Barth, and Y. Yang, "Magnetic Field and Temperature Scaling of the Critical Current of REBCO Tapes," *IEEE Trans. Appl. Supercond.*, vol. 34, no. 3, pp. 1–7, 2024, doi: 10.1109/TASC.2024.3370137.